Anomalous Net Biome Exchange Over Amazonian Rainforests Induced by the 2015/16 El Niño: Soil Dryness-Shaped Spatial Pattern but Temperature-dominated Total Flux

Jun Wang[1,2], Ning Zeng[3], Meirong Wang[2,4], Fei Jiang[1], Frédéric Chevallier[5], Sean Crowell[6], Wei He[1], Matthew S. Johnson[7], Junjie Liu[8], Zhiqiang Liu[9], Scot M. Miller[10], Sajeev Philip[11], Hengmao Wang[1], Mousong Wu[1], Weimin Ju[1], Shuzhuang Feng[1], and Mengwei Jia[1]

[1]Frontiers Science Center for Critical Earth Material Cycling/International Institute for Earth System Science, Nanjing University, Nanjing, China, [2]Key Laboratory of Meteorological Disaster (KLME), Ministry of Education & Collaborative Innovation Center on Forecast and Evaluation of Meteorological Disasters (CIC-FEMD), Nanjing University of Information Science & Technology, Nanjing, China, [3]Department of Atmospheric and Oceanic Science, Earth System Interdisciplinary Center, University of Maryland, College Park, MD, USA, [4]Joint Center for Data Assimilation Research and Applications/Joint International Research Laboratory of Climate and Environment Change (ILCEC), Nanjing University of Information Science and Technology, Nanjing, China, [5]Laboratoire des Sciences du Climat et de L'Environnement, LSCE/IPSL, CEA-CNRS-UVSQ, Université Paris-Saclay, Gif-sur-Yvette, France, [6]University of Oklahoma, Norman, OK, USA, [7]Earth Science Division, NASA Ames Research Center, Moffett Field, CA, USA, [8]Jet Propulsion Laboratory, California Institute of Technology, Pasadena, CA, USA, [9]State Key Laboratory of Numerical Modelling for Atmospheric Sciences and Geophysical Fluid Dynamics, Institute of Atmospheric Physics, Chinese Academy of Sciences, Beijing, China, [10]Department of Environmental Health and Engineering, Johns Hopkins University, Baltimore, MD, USA, [11]Centre for Atmospheric Sciences, Indian Institute of Technology Delhi, New Delhi, India

Abstract The magnitude and spatial pattern of anomalous net biome exchange (NBE) induced by the 2015/16 El Niño over Amazonian rainforests remain uncertain. We here investigated them using multi-model posterior NBE products in the Orbiting Carbon Observatory-2 (OCO-2) version 10 modeling intercomparison project. Results suggest that relative to the annual NBE average in 2017/18, larger anomalous carbon release occurred over the eastern and northern Amazonian rainforests in 2015/16, with a total flux of approximately 0.4 PgC yr^{-1} after assimilating satellite-observed column CO_2 concentrations (XCO_2) over land. We further find that this anomalous spatial pattern was predominantly determined by soil dryness, while the total positive NBE anomaly was dominated by higher temperature with its contribution of approximately 68∼70%. We believe that atmospheric inversions assimilating more satellite-observed XCO_2 in future can provide us more comprehensive understanding how Amazonian rainforests cope with the abiotic stresses induced by El Niño events.

Plain Language Summary Interannual variability of carbon flux associated with its drivers over Amazonian rainforests are not fully understood. We here used several groups' newly available posterior CO_2 flux estimates to comprehensively investigate the net carbon flux anomaly induced by the 2015/16 extreme El Niño. A total net carbon flux anomaly of approximately 0.4 PgC yr^{-1} was estimated, which showed larger carbon release over the eastern and northern Amazonian rainforests. We further suggest that although dry conditions greatly shaped the spatial pattern of the anomalous carbon flux, the total carbon flux anomaly was controlled by the higher temperature, with its contribution of approximately 68∼70%.

1. Introduction

The interannual variability of tropical and global land-atmosphere carbon flux, linked to the El Niño-Southern Oscillation (ENSO), has been a hot topic (Bowman et al., 2017; Jung et al., 2017; Liu et al., 2017; Palmer et al., 2019; Peylin et al., 2013; Piao et al., 2020; Rodenbeck et al., 2018; J. Wang et al., 2016; J. Wang, Zeng, Wang, Jiang, Chen, et al., 2018; Zeng et al., 2005). In particular, these year-to-year variations reveal how terrestrial ecosystems cope with the abiotic stresses induced by ENSO events, and may shed some light on the future changes of terrestrial carbon cycle under greenhouse warming (Arora et al., 2020; Cox et al., 2018; Friedlingstein et al., 2006). The tropical rainforests, with the largest areas located over Amazonia, make the second largest contribution (approximately 28%) to the interannual variability of global net biome productivity based on the

TRENDY multi-model simulations (Ahlstrom et al., 2015). Amazonia has been long recognized as a hot spot of carbon cycle research due to its interannual anomalies (Koren et al., 2018; Phillips et al., 2009; van Schaik et al., 2018) and long-term changes (Cox et al., 2004; Gatti et al., 2021; Green et al., 2020).

During the recent 2015/16 extreme El Niño, the gross primary productivity and solar-induced fluorescence (SIF) were suppressed over Amazonia due to anomalously higher temperature and lower soil moisture (Koren et al., 2018; van Schaik et al., 2018); however, forest canopy greenness showed a small increase due to enhanced solar radiation (Yang et al., 2018). As for the net carbon flux to atmosphere, an inverse modeling study suggested approximately 0.5 PgC release anomaly from Amazonia from September 2015 to June 2016, by assimilating in situ observations and vertical profile data in the Amazon (Gloor et al., 2018). Liu et al. (2017) suggested 0.9 ± 0.29 Pg more carbon into atmosphere in 2015 than in the previous La Niña year 2011 over tropical South America, which was estimated by an atmospheric inversion constrained with CO_2 observations from the Orbiting Carbon Observatory-2 (OCO-2), SIF, and carbon monoxide observations from Measurements of Pollution in the Troposphere. However, these two studies did not show the spatial characteristics of anomalous net land-atmosphere carbon flux, and qualitatively discussed the related climate drivers.

Recently, net biome exchange (NBE) from the OCO-2 version 10 modeling intercomparison project (MIP) have become available. The NBE is sum of net ecosystem exchange (NEE) and wildfire-induced carbon emissions (F_{fire}). We expect that these models can better capture the characteristics of regional carbon flux anomalies after assimilating satellite-observed XCO_2 data, compared with the traditional atmospheric inversions used in previous studies (Bastos et al., 2018; J. Wang, Zeng, Wang, Jiang, Wang, & Jiang, 2018). Therefore, based on the posterior NBE optimized by these multiple inversion models, we revisit the magnitude and spatial pattern of anomalous NBE over Amazonian rainforests induced by the extreme 2015/16 El Niño. Further, we will attempt to quantitatively reveal the effects of different climate drivers.

2. Materials and Methods

2.1. Posterior NBE From Multiple Atmospheric Inversion Models

This study used the NBE products optimized by 13 atmospheric inversion models (Table S1 in Supporting Information S1) from the OCO-2 v10 MIP, which is an international collaboration of CO_2 flux inversion modelers. Modelers performed a standard suit of inversion experiments, constrained by CO_2 observations from OCO-2 and in situ (Byrne et al., 2022; Crowell et al., 2019; Peiro et al., 2022), reported posterior results for years 2015–2020. For each inversion experiment, modelers prescribed a common fossil fuel emission, but independently adopted other prior surface carbon flux estimates (NEE, ocean, and wildfire emissions) (Peiro et al., 2022). The common fossil fuel emission adopted the Open-source Data Inventory for Anthropogenic CO_2 (ODIAC) emission data product with the monthly gridded $1° \times 1°$ emissions up to 2019 (Oda et al., 2018) and extrapolated emissions in 2020 with additional information from the Carbon Monitor emission product (https://carbonmonitor.org/). In this study, we adopted results from three experiments, including: (a) IS: Assimilation of in situ CO_2 measurements from an international observational network; (b) LNLG: Assimilation of OCO-2 ACOS v10 land nadir and land glint XCO_2 retrievals (OCO-2 Science Team/Gunson & Eldering, 2020); (c) LNLGIS: Assimilation of in situ CO_2 measurements and OCO-2 ACOS v10 land nadir and land glint XCO_2 retrievals.

Taking the inter-model spread into account, we made a simple screening of the models over the Amazonian rainforests by using the Kling-Gupta Efficiency (KGE) (Gupta et al., 2009; Kling et al., 2012):

$$\text{KGE}(y, \hat{y}) = 1 - \sqrt{(r(y, \hat{y}) - 1)^2 + (\beta(y, \hat{y}) - 1)^2 + (\gamma(y, \hat{y}) - 1)^2} \tag{1}$$

where y and $\hat{y}$ here represent the reference and simulated total NBE fluxes, respectively. The term of $r(y, \hat{y})$ shows their Pearson's correlation coefficient, $\beta(y, \hat{y})$ the bias ratio, and $\gamma(y, \hat{y})$ the variability ratio. We can derive $\beta(y, \hat{y})$ and $\gamma(y, \hat{y})$ as follows:

$$\begin{cases} \beta(y, \hat{y}) = \dfrac{\mu_{\hat{y}}}{\mu_y} \\ \gamma(y, \hat{y}) = \dfrac{\sigma_{\hat{y}}/\mu_{\hat{y}}}{\sigma_y/\mu_y} \end{cases} \tag{2}$$

where μ represents the mean, and σ the standard deviation. Clearly, the range of KGE is $(-\text{inf},1]$, with the best possible score of 1 when the simulated result is exactly equal to the reference.

The posterior NBE was provided by the OCO-2 v10 MIP community at $1° \times 1°$. In order to lower the noise in space to some extent, we in this study performed the analyses at $2.5° \times 2.5°$ which were interpolated by using the Climate Data Operators tool based on the approach of the first order conservative remapping scheme (Jones, 1999):

$$\overline{F_k} = \frac{1}{A_k} \iint f \, dA \tag{3}$$

where $\overline{F_k}$ represents the area-averaged destination terrestrial carbon flux, A_k the area of grid k, and f the original carbon flux.

2.2. Meteorological and Land Cover Data Sets

The soil dryness condition here was indicated by the terrestrial water storage (TWS) from a reconstructed product of the Gravity Recovery and Climate Experiment (GRACE-REC) which was generated by a statistical model trained with GRACE observations (Humphrey & Gudmundsson, 2019). The GRACE-REC product was provided in six reconstructed TWS data sets of 100 ensemble members each at both daily and monthly timesteps over the period of 1901 to present with a $0.5° \times 0.5°$ resolution, based on two different GRACE products (JPL and GSFC mascons) and three meteorological forcing data sets. Considering the time span and product evaluation (Humphrey et al., 2021), this study adopted the ensemble mean of the GSFC-ERA5 monthly product which had the time span from January 1979 to July 2019. In order to independently assess this product, we further compared it with other three soil moisture products, and found that they consistently have high spatial correlation coefficients in pairs over Amazonian rainforests (Table S2 in Supporting Information S1).

We adopted the surface air temperature at 2 m and calculated the vapor pressure deficit (VPD) based on the ERA5 data on single levels at $0.25° \times 0.25°$ (Hersbach et al., 2020). Specifically, we first calculated VPD hourly according to the Tetens' formula for temperature above 0°C (Monteith & Unsworth, 2007):

$$\text{VPD} = 0.61078 \times \left(e^{\frac{17.27 T_{as}}{T_{as}+237.29}} - e^{\frac{17.27 T_d}{T_d+237.29}} \right) \tag{4}$$

where T_{as} and T_d are surface air temperature and dew-point temperature in degrees Celsius, respectively. The derived VPD is in kilopascals (kPa). Then we aggregated calculated hourly VPD into monthly and annual averages.

The Oceanic Niño Index (ONI) was adopted here to infer the ENSO conditions, which was the running 3-month area-averaged sea surface temperature anomalies for the Niño3.4 region (5°S–5°N, 120°–170°W).

In order to retrieve the domain of Amazonian rainforests (evergreen broadleaf forests) in this study, we adopted the Terra and Aqua combined Moderate Resolution Imaging Spectroradiometer (MODIS) Land Cover Climate Modeling Grid (MCD12C1) Version 6 data product (Friedl & Sulla-Menashe, 2015), which were also consistently resampled into $2.5° \times 2.5°$ by the approach of the largest area fraction remapping (Figure S1 in Supporting Information S1).

2.3. Calculation of NBE and Climate Anomalies

According to the ONI table, an extreme El Niño occurred in 2015/16 with the maximum ONI of 2.6°C, followed by two weak La Niña events in 2016/17 and 2017/18. Owing to the short period of posterior NBE products, the climatology cannot be accurately derived which can be greatly influenced by the extreme El Niño event. Hence, we derived the anomalies of NBE and climate factors in each grid over Amazonian rainforests by calculating the difference between the averages during 2015/16 and those during 2017/18. It is similar to the approach of Liu et al. (2017) in which they calculated the anomaly in 2015 relative to the value in 2011.

2.4. Contributions of Climate Drivers to NBE Anomalies

Surface air temperature, soil moisture, and VPD are the main climate factors, driving the interannual variability of land-atmosphere carbon flux (He et al., 2022; Humphrey et al., 2018; Jung et al., 2017; J. Wang et al., 2016;

W. Wang et al., 2013). In order to quantitatively derive the contributions of these three climate drivers to NBE anomalies over Amazonian rainforests, we calculated their pattern correlation coefficients and adopted the multiple linear regression model to apparently decompose NBE anomalies which has been widely used in previous studies (Dannenberg et al., 2022; Humphrey et al., 2021; Jung et al., 2017).

Specifically, decomposition of NBE anomalies into individual contributions was achieved as follows:

$$\text{NBE} = \alpha^T T + \alpha^{\text{TWS}}\text{TWS} + \alpha^{\text{VPD}}\text{VPD} + \varepsilon \tag{5}$$

where α^T, α^{TWS}, and α^{VPD} represent the sensitivities of NBE to temperature, TWS, and VPD anomalies, respectively. The term of ε represents the residual. We can further rewrite Equation 5 using the more compact symbols:

$$\text{NBE} = \text{NBE}^T + \text{NBE}^{\text{TWS}} + \text{NBE}^{\text{VPD}} + \varepsilon \tag{6}$$

where NBE^T, NBE^{TWS}, and NBE^{VPD} denote the NBE anomalies induced by temperature, TWS, and VPD, respectively. In addition, we randomly combined two of these three climate drivers to linearly decompose NBE anomalies in the same way, so as to comprehensively understand the contributions of climate drivers to the total NBE anomaly.

3. Results

3.1. Performance of Inversion Models

Although these inversion models assimilated the same CO_2 observations and followed the same protocols, large inter-model spreads still existed in the posterior NBE (Byrne et al., 2022; Crowell et al., 2019; Peiro et al., 2022) which can be caused by the settings for errors in prior surface carbon fluxes, the errors in the atmospheric transport induced by different transport models and meteorological products used, and choices in the optimization techniques (Table S1 in Supporting Information S1) (Basu et al., 2018; Chevallier et al., 2010; Schuh et al., 2019). Hence, we conducted a simple model screening here. First, we calculated the total posterior NBE over the Amazonian rainforests for each inversion model in the period of 2015–2018. Second, taking the inverted total net carbon flux from Gatti et al. (2021) (denoted as "Gatti2021") which was estimated based on 590 aircraft vertical profiling measurements of lower-tropospheric CO_2 and CO concentrations at four sites in Amazonia as the reference, we calculated their correlation, bias, and variability in the same period to derive the KGE scores for each model (Equation 1). We can find that most of models show big KGE scores in LNLG and LNLGIS experiments, indicating that the posterior NBE in these models are consistent with the Gatti2021. Taking the mean flow benchmark (KGE = −0.41) (Knoben et al., 2019) as the threshold, we screened out Baker (KGE = −7.58 in LNLG and −6.67 in LNLGIS) and CMS-Flux (KGE = −4.83 in LNLG and −1.65 in LNLGIS) models so as to make the multi-model ensemble (MME) to perform the following analyses. And the resulting MME shows the KGE of 0.48 in LNLG and 0.59 in LNLGIS, respectively.

3.2. Anomalous Posterior NBE Over Amazonian Rainforests

The geographical distributions of calculated annual NBE anomalies over Amazonian rainforests related to the extreme 2015/16 El Niño are presented in Figure 2. The ensemble NBE anomalies in OCO-2 v10 MIP Prior were nearly neutral (Figure 2a), which suggested that the obvious posterior NBE anomalies in IS, LNLG, and LNLGIS experiments originated from the information of the in situ and satellite-observed atmospheric CO_2 concentrations (Figures 2b–2d). In detail, the ensemble NBE anomalies constrained by in situ CO_2 observations (IS experiment) showed moderate anomalous carbon release (positive values) with the slightly stronger magnitudes over the eastern Amazonia (Figure 2b). Compared to the limited stations of in situ CO_2 observations (Figure 2b), the OCO-2 XCO_2 product largely increases the coverage of atmospheric CO_2 observations over the tropical South America (Figure 2c). The ensemble posterior NBE anomalies in LNLG and LNLGIS had the similar spatial patterns, showing the much stronger carbon release over the eastern and northern parts of Amazonian rainforests (Figures 2c and 2d). More detailed spatial characteristics of posterior NBE anomalies for each model in LNLG and LNLGIS can be referred to in Figures S2 and S3 of Supporting Information S1.

More specifically, longitudinal changes of NBE anomalies showed that although large inter-model spread existed, the ensemble posterior NBE anomalies in LNLG and LNLGIS had significantly stronger carbon release
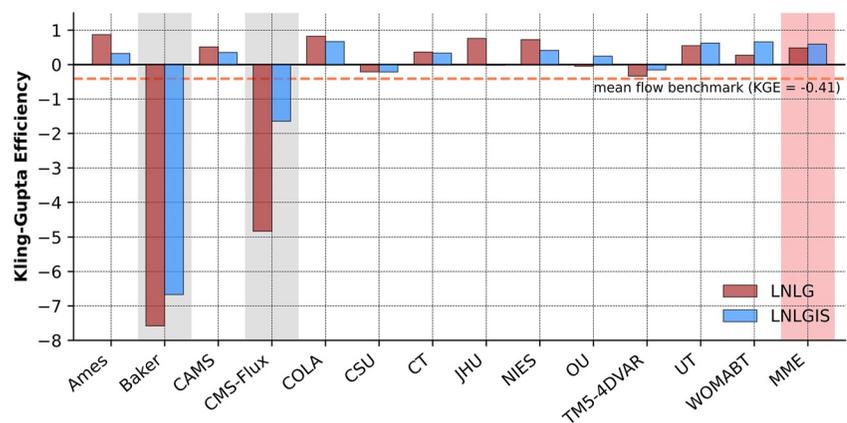
Figure 1. Kling-Gupta Efficiency (KGE) for each inversion model involved in the OCO-2 v10 modeling intercomparison project. Because there are no direct large-scale observations for the net biome exchange over Amazonian rainforests, we adopted results from Gatti et al. (2021) as the reference. The KGE was calculated for the period of 2015–2018 with the mean flow benchmark (KGE = −0.41) as the threshold.

(approximately double, >0.05 PgC yr^{-1}) from 57.5°W to 67.5°W than results in IS ($p < 0.1$) (Figure 2e). The ensemble NBE anomalies over the entire Amazonian rainforests were 0.03 ± 0.07 PgC yr^{-1} in Prior and 0.29 ± 0.23 PgC yr^{-1} in IS. After assimilating OCO-2 XCO$_2$ land nadir and glint observations, the total ensemble NBE anomalies were 0.43 ± 0.14 PgC yr^{-1} in LNLG and 0.40 ± 0.16 PgC yr^{-1} in LNLGIS, showing their enhanced carbon release by approximately 48% and 38%, respectively, relative to the estimated magnitude in IS. The magnitudes of these ensemble NBE anomalies in LNLG and LNLGIS were closer to that of Gatti2021 with its value of 0.48 PgC yr^{-1} (Figure 1f). Hence, we will focus on the results in LNLG and LNLGIS in the following text. The NBE anomaly composed of NEE and F_{fire} anomalies, in which F_{fire} anomaly was estimated at 0.05 PgC yr^{-1} based on GFEDv4.1s product (Figure 1f), suggesting that the dominant contributor to the NBE anomaly is NEE. Additionally, the inter-model spread in the total NBE anomalies in IS was larger than that in LNLG, indicating that larger discrepancies existed in assimilating in situ observations in these atmospheric inversion models.

3.3. Anomalous Pattern-Related Climate Drivers

Interannual NBE anomalies were predominantly controlled by temperature, soil moisture, and VPD, as suggested by previous studies (He et al., 2022; Humphrey et al., 2018; Jung et al., 2017; J. Wang et al., 2016; W. Wang et al., 2013; Zeng et al., 2005). Regression analysis revealed that 1K increase of ONI in the preceding December can increase the annual temperature by 0.34 K ($R^2 = 0.35$, $p < 0.05$), enhance VPD by 0.02 kPa ($R^2 = 0.41$, $p < 0.05$), and reduce TWS by 0.16 TtH$_2$O ($R^2 = 0.84$, $p < 0.05$) over the entire Amazonian rainforests (Figure 3a). Accordingly, the climate condition showed the higher temperature and VPD and drier soil in 2015/16, whereas it had the lower temperature and VPD and wetter soil in 2017/18 (Figure 3a). Relative to the averages in 2017/18, higher temperature occurred over the entire Amazonian rainforests (Figure 3b), which can potentially inhibit the vegetation photosynthesis and enhance soil respiration (Crowther et al., 2016; Zeng et al., 2005). The soil and atmospheric dryness mainly occurred over the northeastern Amazonia albeit with some differences in their spatial patterns (Figures 3c and 3d), which both can reduce vegetation photosynthesis (Lopez et al., 2021; Stocker et al., 2019; Werner et al., 2021; Yuan et al., 2019). Therefore, these three climate drivers simultaneously contributed to the positive NBE anomalies (Figures 2c and 2d).

In space, the stronger positive ensemble NBE anomalies over the eastern and northern parts of Amazonian rainforests (Figures 2c and 2d) were visually more consistent with the pattern of TWS anomaly (Figure 3c). Quantitatively, we find that the gridded NBE anomalies were significantly negatively correlated with TWS with the spatial correlation coefficients of −0.51 (confidence interval, CI from −0.65 to −0.33, $p < 0.05$) in LNLG and −0.64 (CI from −0.74 to −0.5, $p < 0.05$) in LNLGIS, respectively. In contrast, they were significantly positively correlated with VPD with the coefficients of 0.48 (CI from 0.31 to 0.62, $p < 0.05$) in LNLG and 0.54 (CI from 0.38 to 0.67, $p < 0.05$) in LNLGIS, respectively (Figure 4a). Although the patterns of TWS and VPD anomalies show similarity (−0.70 with the CI from −0.80 to −0.56, $p < 0.05$) (Figures 3c and 3d), the higher coefficients
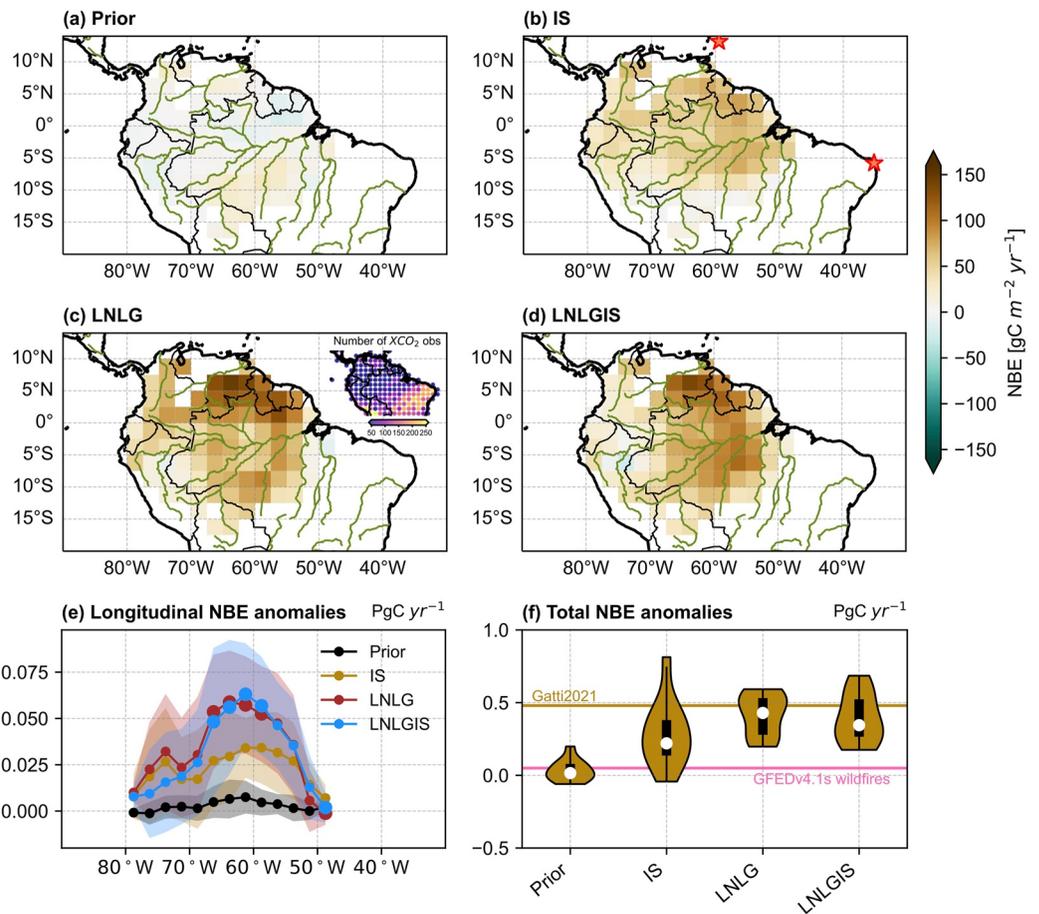
Figure 2. Geographical distributions of anomalous annual net biome exchange (NBE) induced by the 2015/16 El Niño over the Amazonian rainforests. Prior (a) and posterior ensemble NBE anomalies at $2.5° \times 2.5°$ in inversion experiments of IS (b), LNLG (c), and LNLGIS (d) in the OCO-2 v10 modeling intercomparison project. The unit of NBE anomalies in (a–d) is gC m^{-2} yr^{-1}. The red stars in (b) and inserted subplot in (c) show the locations of in situ observations and number of OCO-2 LNLG observations during 2015–2018 in this domain, respectively. (e) Longitudinal total ensemble NBE anomalies in the unit of PgC yr^{-1}. The shaded areas represent the standard deviation ($1-\sigma$) of multi-model inversion results in each experiment. The bigger dots in LNLG and LNLGIS represent that they are significantly different from those in IS with statistical significance at $p < 0.1$ level estimated by the Wilcoxon signed-rank test (Wilcoxon, 1945). (f) Violin and boxplots of multi-model total NBE anomalies over entire Amazonia rainforests. The total NBE is in PgC yr^{-1}. The pink and darkgoldenrod lines represent anomalous carbon emissions induced by wildfires estimated by the GFEDv4.1s data set and anomalous NBE estimated by Gatti2021.

between NBE and TWS suggested the dominant role of TWS in shaping the NBE anomalous pattern related to the extreme 2015/16 El Niño.

3.4. Total NBE Anomaly-Related Climate Drivers

In addition, we conducted the linear decomposition analysis (Equations 5 and 6) to understand which climate driver mostly contributed to the total NBE anomaly over the entire Amazonian rainforests (Figure 4b). We revealed that the total NBE anomaly of 0.43 ± 0.14 PgC yr^{-1} in LNLG composed of 0.30 ± 0.24 PgC yr^{-1} induced by temperature, 0.10 ± 0.12 PgC yr^{-1} induced by TWS, and 0.03 ± 0.15 PgC yr^{-1} induced by VPD, respectively, with the approximately 70% contribution from temperature (Figure 4b). Similarly, the total NBE anomaly of 0.40 ± 0.16 PgC yr^{-1} in LNLGIS was predominantly contributed to by temperature-induced anomaly of 0.27 ± 0.22 PgC yr^{-1} with the approximately 68% contribution.

Furthermore, we randomly combined two of these three climate drivers (three different combinations) to perform the same linear decomposition for NBE anomaly (Figure 4c). When we choose temperature and TWS (or VPD) as
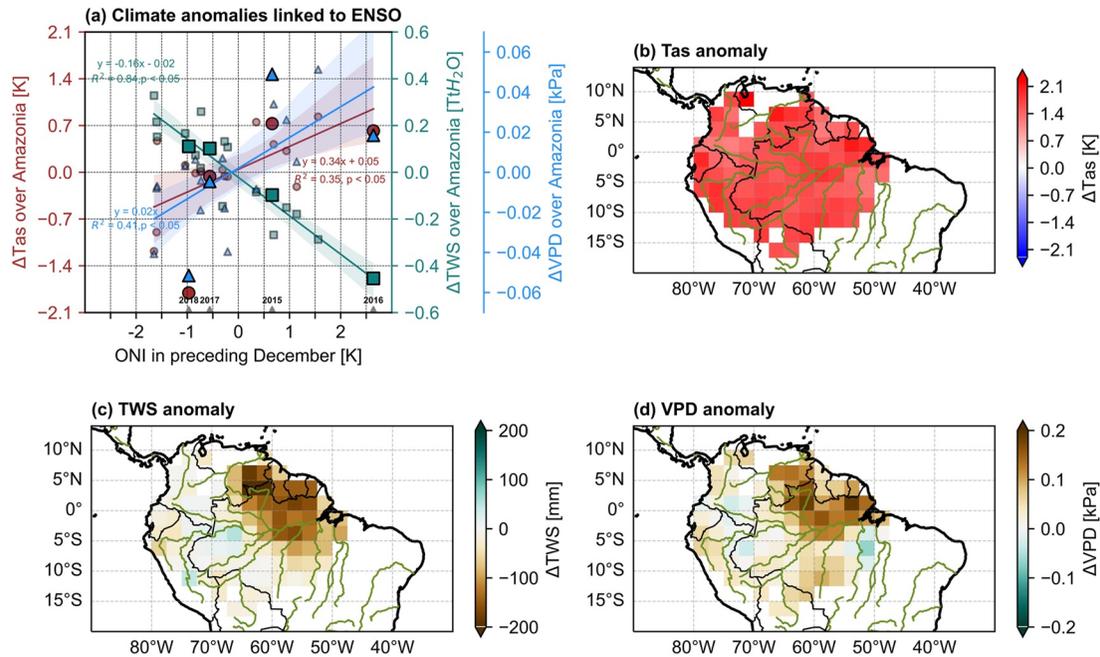
Figure 3. Anomalous climate drivers over the Amazonian rainforests. (a) Relationship between detrended annual climate anomalies, including surface air temperature (Tas, red), terrestrial water storage (TWS, green), and vapor pressure deficit (VPD, blue), and Oceanic Niño Index in the preceding December from 2000 to 2018. The bigger markers represent the values in 2015, 2016, 2017, and 2018, which are denoted at x-axis. Anomalous climate patterns of (b) Tas, (c) TWS, and (d) VPD linked to the 2015/16 El Niño were consistently calculated by their differences between annual mean during 2015–2016 and that during 2017–2018.
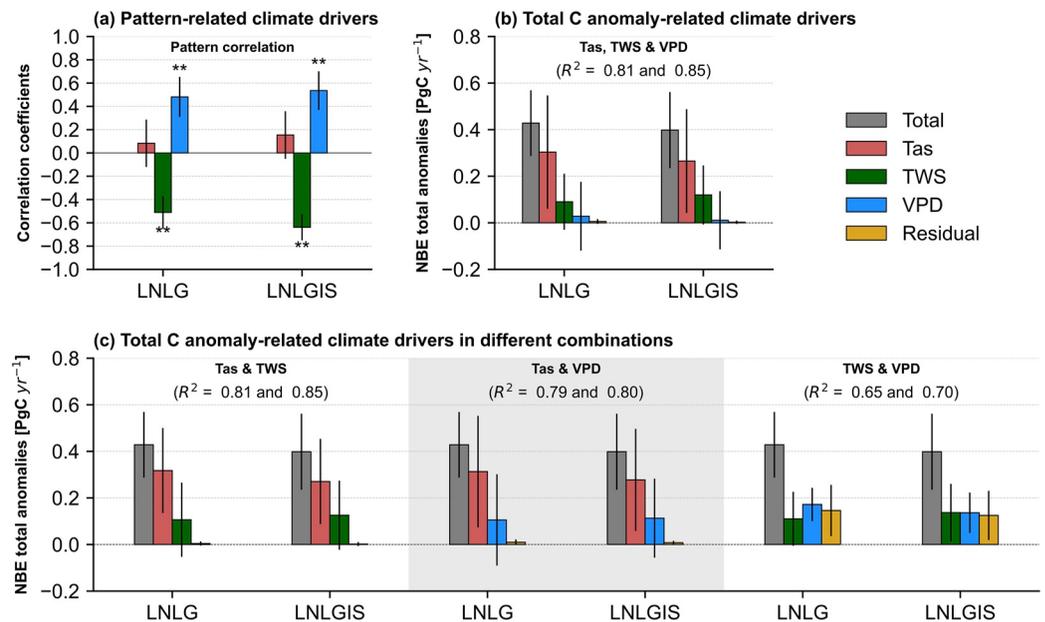

Figure 4. Associations between ensemble annual net biome exchange (NBE) anomalies and climate drivers over Amazonian rainforests. (a) Spatial correlation coefficients between ensemble annual NBE anomalies and individual climate factor. The error bars represent 95% confidence intervals derived by 10,000 bootstrap estimates. The symbol of ** denotes the statistical significance at $p < 0.05$ level. (b and c) Linearly decomposed contributions of individual climate factors to total NBE anomalies induced by the 2015/16 El Niño over entire Amazonian rainforests, based on different combinations. The error bars represent the 1-σ of multi-model inversion results.

the two regressors, the regression models show the comparable performance as the linear decomposition in Equations 5 and 6, with the R^2 in the range of 0.79–0.85 (Figure 4c). Importantly, the decomposed NBE anomaly induced by temperature consistently made the larger contribution to the total NBE anomaly, accounting for approximately 73%–74% in LNLG and 68%–70% in LNLGIS, respectively. And TWS and VPD here accounted for nearly the same fraction of contribution (approximately 25% in LNLG and 30% in LNLGIS, respectively), which were caused by their similarity between TWS and VPD anomalous patterns (Figures 3c and 3d). In contrast, when we selected TWS and VPD to decompose the NBE anomaly, the magnitude of R^2 obviously decreased and the residual term showed large values. It laterally indicated the important contribution of temperature to the total NBE anomalies.

4. Discussion

We here find that the anomalous spatial pattern induced by the extreme 2015/16 El Niño was predominantly determined by soil dryness, while the total positive NBE anomaly was dominated by higher temperature. It is worth mentioning that uncertainty may exist when we derived the individual contributions of different climate drivers through the linear decomposition upon the spatial NBE anomalies. For instance, (a) we potentially assumed the homogeneous climate sensitivities of Amazonian rainforests. However, although we focus on the consistent broadleaf forest on the basis of MODIS landcover, the uneven forest composition at the landscape level (topographic highs and lows) and along the precipitation gradient (Fancourt et al., 2022; Wittmann et al., 2006) can to some extent make our assumption inadequate. (b) Different climate drivers are not independent (Figure 3). In order to assess the impact of their interactions on the linear decomposition, we added some interaction terms (Equation S1 in Supporting Information S1) to further decompose their individual contributions (Luo et al., 2021). Although we agree that it is not strictly a nonlinear model yet because the dependence on the individual drivers is still of first order and it does not fully represent the complex soil-plant-atmosphere interactions, the contributions from those interaction terms are small and the derived temperature contributions are approximately 74% in LNLG and 70% in LNLGIS (Figure S4 in Supporting Information S1), which are consistent with the results derived by Equations 5 and 6. (c) Climate products have uncertainties in anomalous pattern and strength (Figure 3 and Figure S5 in Supporting Information S1). To further test the robustness of the results, we conducted the same analysis using the temperature and derived VPD (Equation S2 in Supporting Information S1) from the Climatic Research Unit gridded Time Series (CRU TS) v.4.05 product (Harris et al., 2020), and found that the main conclusion remained the same (Figure S6 in Supporting Information S1). Therefore, we believe that the results here are credible albeit the uncertainties are inevitable.

So what causes the inconsistency in the dominant climate drivers for NBE anomalous pattern and total flux over the rainforests? Actually, we think that this difference greatly links to the spatial scales of anomalous temperature and soil water, as discussed by Jung et al. (2017). Although it does not turn out the compensatory water effect here, the area of higher temperature is much larger than that of soil dryness (Figures 3b and 3c). This difference in spatial scale leads to the fact that the total NBE anomaly was not controlled by soil water availability, but by temperature. Results here suggest that it is necessary to distinguish the climate drivers for anomalous pattern and total flux of carbon in order to comprehensively understand how the abiotic stresses influence the regional carbon cycle.

Conflict of Interest

The authors declare no conflicts of interest relevant to this study.

Data Availability Statement

References

Ahlstrom, A., Raupach, M. R., Schurgers, G., Smith, B., Arneth, A., Jung, M., et al. (2015). The dominant role of semi-arid ecosystems in the trend and variability of the land CO_2 sink. *Science*, *348*(6237), 895–899. https://doi.org/10.1126/science.aaa1668

Arora, V. K., Katavouta, A., Williams, R. G., Jones, C. D., Brovkin, V., Friedlingstein, P., et al. (2020). Carbon–concentration and carbon–climate feedbacks in CMIP6 models and their comparison to CMIP5 models. *Biogeosciences*, *17*(16), 4173–4222. https://doi.org/10.5194/bg-17-4173-2020

Bastos, A., Friedlingstein, P., Sitch, S., Chen, C., Mialon, A., Wigneron, J. P., et al. (2018). Impact of the 2015/2016 El Nino on the terrestrial carbon cycle constrained by bottom-up and top-down approaches. *Philosophical Transactions of the Royal Society of London Series B Biological Sciences*, *373*(1760), 20170304. https://doi.org/10.1098/rstb.2017.0304

Basu, S., Baker, D. F., Chevallier, F., Patra, P. K., Liu, J., & Miller, J. B. (2018). The impact of transport model differences on CO_2 surface flux estimates from OCO-2 retrievals of column average CO_2. *Atmospheric Chemistry and Physics*, *18*(10), 7189–7215. https://doi.org/10.5194/acp-18-7189-2018

Bowman, K. W., Liu, J., Bloom, A. A., Parazoo, N. C., Lee, M., Jiang, Z., et al. (2017). Global and Brazilian carbon response to El Niño Modoki 2011–2010. *Earth and Space Science*, *4*(10), 637–660. https://doi.org/10.1002/2016ea000204

Byrne, B., Baker, D. F., Basu, S., Bertolacci, M., Bowman, K. W., Carroll, D., et al. (2022). National CO_2 budgets (2015–2020) inferred from atmospheric CO_2 observations in support of the global stocktake. *Earth System Science Data Discussions*, *2022*, 1–59.

Chevallier, F., Feng, L., Bösch, H., Palmer, P. I., & Rayner, P. J. (2010). On the impact of transport model errors for the estimation of CO_2 surface fluxes from GOSAT observations. *Geophysical Research Letters*, *37*(21), L21803. https://doi.org/10.1029/2010gl044652

Cox, P. M., Betts, R. A., Collins, M., Harris, P. P., Huntingford, C., & Jones, C. D. (2004). Amazonian forest dieback under climate-carbon cycle projections for the 21st century. *Theoretical and Applied Climatology*, *78*(1–3), 137–156. https://doi.org/10.1007/s00704-004-0049-4

Cox, P. M., Huntingford, C., & Williamson, M. S. (2018). Emergent constraint on equilibrium climate sensitivity from global temperature variability. *Nature*, *553*(7688), 319–322. https://doi.org/10.1038/nature25450

Crowell, S., Baker, D., Schuh, A., Basu, S., Jacobson, A. R., Chevallier, F., et al. (2019). The 2015–2016 carbon cycle as seen from OCO-2 and the global in situ network. *Atmospheric Chemistry and Physics*, *19*(15), 9797–9831. https://doi.org/10.5194/acp-19-9797-2019

Crowther, T. W., Todd-Brown, K. E., Rowe, C. W., Wieder, W. R., Carey, J. C., Machmuller, M. B., et al. (2016). Quantifying global soil carbon losses in response to warming. *Nature*, *540*(7631), 104–108. https://doi.org/10.1038/nature20150

Dannenberg, M. P., Yan, D., Barnes, M. L., Smith, W. K., Johnston, M. R., Scott, R. L., et al. (2022). Exceptional heat and atmospheric dryness amplified losses of primary production during the 2020 U.S. Southwest hot drought. *Global Change Biology*, *28*(16), 4794–4806. https://doi.org/10.1111/gcb.16214

Fancourt, M., Ziv, G., Boersma, K. F., Tavares, J., Wang, Y., & Galbraith, D. (2022). Background climate conditions regulated the photosynthetic response of Amazon forests to the 2015/2016 El Nino-Southern Oscillation event. *Communications Earth & Environment*, *3*(1), 209. https://doi.org/10.1038/s43247-022-00533-3

Friedl, M., & Sulla-Menashe, D. (2015). MCD12C1 MODIS/Terra+Aqua Land Cover Type Yearly L3 Global 0.05Deg CMG V006 [Dataset]. NASA EOSDIS Land Processes DAAC. https://doi.org/10.5067/MODIS/MCD12C1.006

Friedlingstein, P., Cox, P., Betts, R., Bopp, L., von Bloh, W., Brovkin, V., et al. (2006). Climate-carbon cycle feedback analysis: Results from the C^4MIP model intercomparison. *Journal of Climate*, *19*(14), 3337–3353. https://doi.org/10.1175/jcli3800.1

Gatti, L. V., Basso, L. S., Miller, J. B., Gloor, M., Gatti Domingues, L., Cassol, H. L., et al. (2021). Amazonia as a carbon source linked to deforestation and climate change. *Nature*, *595*(7867), 388–393. https://doi.org/10.1038/s41586-021-03629-6

Gloor, E., Wilson, C., Chipperfield, M. P., Chevallier, F., Buermann, W., Boesch, H., et al. (2018). Tropical land carbon cycle responses to 2015/16 El Nino as recorded by atmospheric greenhouse gas and remote sensing data. *Philosophical Transactions of the Royal Society of London Series B: Biological Sciences*, *373*(1760), 20170302. https://doi.org/10.1098/rstb.2017.0302

Green, J. K., Berry, J., Ciais, P., Zhang, Y., & Gentine, P. (2020). Amazon rainforest photosynthesis increases in response to atmospheric dryness. *Science Advances*, *6*(47), eabb7232. https://doi.org/10.1126/sciadv.abb7232

Gupta, H. V., Kling, H., Yilmaz, K. K., & Martinez, G. F. (2009). Decomposition of the mean squared error and NSE performance criteria: Implications for improving hydrological modelling. *Journal of Hydrology*, *377*(1–2), 80–91. https://doi.org/10.1016/j.jhydrol.2009.08.003

Harris, I., Osborn, T. J., Jones, P., & Lister, D. (2020). Version 4 of the CRU TS monthly high-resolution gridded multivariate climate dataset. *Scientific Data*, *7*(1), 109. https://doi.org/10.1038/s41597-020-0453-3

He, B., Chen, C., Lin, S., Yuan, W., Chen, H. W., Chen, D., et al. (2022). Worldwide impacts of atmospheric vapor pressure deficit on the interannual variability of terrestrial carbon sinks. *National Science Review*, *9*(4), nwab150. https://doi.org/10.1093/nsr/nwab150

Hersbach, H., Bell, B., Berrisford, P., Hirahara, S., Horányi, A., Muñoz-Sabater, J., et al. (2020). The ERA5 global reanalysis. *Quarterly Journal of the Royal Meteorological Society*, *146*(730), 1999–2049. https://doi.org/10.1002/qj.3803

Humphrey, V., Berg, A., Ciais, P., Gentine, P., Jung, M., Reichstein, M., et al. (2021). Soil moisture–atmosphere feedback dominates land carbon uptake variability. *Nature*, *592*(7852), 65–69. https://doi.org/10.1038/s41586-021-03325-5

Humphrey, V., & Gudmundsson, L. (2019). GRACE-REC: A reconstruction of climate-driven water storage changes over the last century. *Earth System Science Data*, *11*(3), 1153–1170. https://doi.org/10.5194/essd-11-1153-2019

Humphrey, V., Zscheischler, J., Ciais, P., Gudmundsson, L., Sitch, S., & Seneviratne, S. I. (2018). Sensitivity of atmospheric CO_2 growth rate to observed changes in terrestrial water storage. *Nature*, *560*(7720), 628–631. https://doi.org/10.1038/s41586-018-0424-4

Jones, P. W. (1999). First- and second-order conservative remapping schemes for grids in spherical coordinates. *Monthly Weather Review*, *127*(9), 2204–2210. https://doi.org/10.1175/1520-0493(1999)127<2204:fasocr>2.0.co;2

Jung, M., Reichstein, M., Schwalm, C. R., Huntingford, C., Sitch, S., Ahlström, A., et al. (2017). Compensatory water effects link yearly global land CO_2 sink changes to temperature. *Nature*, *541*(7638), 516–520. https://doi.org/10.1038/nature20780

Kling, H., Fuchs, M., & Paulin, M. (2012). Runoff conditions in the upper Danube basin under an ensemble of climate change scenarios. *Journal of Hydrology*, *424*, 264–277. https://doi.org/10.1016/j.jhydrol.2012.01.011

Knoben, W. J. M., Freer, J. E., & Woods, R. A. (2019). Technical note: Inherent benchmark or not? Comparing Nash–Sutcliffe and Kling–Gupta efficiency scores. *Hydrology and Earth System Sciences*, *23*(10), 4323–4331. https://doi.org/10.5194/hess-23-4323-2019

Koren, G., van Schaik, E., Araújo, A. C., Boersma, K. F., Gärtner, A., Killaars, L., et al. (2018). Widespread reduction in sun-induced fluorescence from the Amazon during the 2015/2016 El Nino. *Philosophical Transactions of the Royal Society of London Series B Biological Sciences*, *373*(1760), 20170408. https://doi.org/10.1098/rstb.2017.0408

Liu, J., Bowman, K. W., Schimel, D. S., Parazoo, N. C., Jiang, Z., Lee, M., et al. (2017). Contrasting carbon cycle responses of the tropical continents to the 2015–2016 El Nino. *Science*, *358*(6360). https://doi.org/10.1126/science.aam5690

Lopez, J., Way, D. A., & Sadok, W. (2021). Systemic effects of rising atmospheric vapor pressure deficit on plant physiology and productivity. *Global Change Biology*, *27*(9), 1704–1720. https://doi.org/10.1111/gcb.15548

Luo, X., Keenan, T. F., Chen, J. M., Croft, H., Colin Prentice, I., Smith, N. G., et al. (2021). Global variation in the fraction of leaf nitrogen allocated to photosynthesis. *Nature Communications*, *12*(1), 4866. https://doi.org/10.1038/s41467-021-25163-9

Monteith, J. L., & Unsworth, M. H. (2007). *Principles of environmental physics* (3rd ed.). Academic Press.

OCO-2 Science Team/Gunson, M., & Eldering, A. (2020). *OCO-2 Level 2 bias-corrected XCO$_2$ and other select fields from the full-physics retrieval aggregated as daily files, Retrospective processing V10r*. Goddard Earth Sciences Data and Information Services Center (GES DISC). https://doi.org/10.5067/E4E140XDMPO2

Oda, T., Maksyutov, S., & Andres, R. J. (2018). The Open-source data Inventory for Anthropogenic CO$_2$, version 2016 (ODIAC2016): A global monthly fossil fuel CO$_2$ gridded emissions data product for tracer transport simulations and surface flux inversions. *Earth System Science Data*, *10*(1), 87–107. https://doi.org/10.5194/essd-10-87-2018

Palmer, P. I., Feng, L., Baker, D., Chevallier, F., Bosch, H., & Somkuti, P. (2019). Net carbon emissions from African biosphere dominate pan-tropical atmospheric CO$_2$ signal. *Nature Communications*, *10*(1), 3344. https://doi.org/10.1038/s41467-019-11097-w

Peiro, H., Crowell, S., Schuh, A., Baker, D. F., O'Dell, C., Jacobson, A. R., et al. (2022). Four years of global carbon cycle observed from the Orbiting Carbon Observatory 2 (OCO-2) version 9 and in situ data and comparison to OCO-2 version 7. *Atmospheric Chemistry and Physics*, *22*(2), 1097–1130. https://doi.org/10.5194/acp-22-1097-2022

Peylin, P., Law, R. M., Gurney, K. R., Chevallier, F., Jacobson, A. R., Maki, T., et al. (2013). Global atmospheric carbon budget: Results from an ensemble of atmospheric CO$_2$ inversions. *Biogeosciences*, *10*(10), 6699–6720. https://doi.org/10.5194/bg-10-6699-2013

Philip, S., Johnson, M. S., Baker, D. F., Basu, S., Tiwari, Y. K., Indira, N. K., et al. (2022). OCO-2 satellite-Imposed constraints on terrestrial biospheric CO$_2$ fluxes Over South Asia. *Journal of Geophysical Research: Atmospheres*, *127*(3), e2021JD035035. https://doi.org/10.1029/2021jd035035

Piao, S. L., Wang, X. H., Wang, K., Li, X. Y., Bastos, A., Canadell, J. G., et al. (2020). Interannual variation of terrestrial carbon cycle: Issues and perspectives. *Global Change Biology*, *26*(1), 300–318. https://doi.org/10.1111/gcb.14884

Rodenbeck, C., Zaehle, S., Keeling, R., & Heimann, M. (2018). History of El Nino impacts on the global carbon cycle 1957–2017: A quantification from atmospheric CO$_2$ data. *Philosophical Transactions of the Royal Society of London Series B Biological Sciences*, *373*(1760), 20170303. https://doi.org/10.1098/rstb.2017.0303

Schuh, A. E., Jacobson, A. R., Basu, S., Weir, B., Baker, D., Bowman, K., et al. (2019). Quantifying the impact of atmospheric transport uncertainty on CO$_2$ surface flux estimates. *Global Biogeochemical Cycles*, *33*(4), 484–500. https://doi.org/10.1029/2018gb006086

Stocker, B. D., Zscheischler, J., Keenan, T. F., Prentice, I. C., Seneviratne, S. I., & Peñuelas, J. (2019). Drought impacts on terrestrial primary production underestimated by satellite monitoring. *Nature Geoscience*, *12*(4), 264–270. https://doi.org/10.1038/s41561-019-0318-6

van Schaik, E., Killaars, L., Smith, N. E., Koren, G., van Beek, L. P. H., Peters, W., & van der Laan-Luijkx, I. T. (2018). Changes in surface hydrology, soil moisture and gross primary production in the Amazon during the 2015/2016 El Nino. *Philosophical Transactions of the Royal Society of London Series B: Biological Sciences*, *373*(1760), 20180084. https://doi.org/10.1098/rstb.2018.0084

Wang, J., Zeng, N., & Wang, M. (2016). Interannual variability of the atmospheric CO$_2$ growth rate: Roles of precipitation and temperature. *Biogeosciences*, *13*(8), 2339–2352. https://doi.org/10.5194/bg-13-2339-2016

Wang, J., Zeng, N., Wang, M., Jiang, F., Chen, J., Friedlingstein, P., et al. (2018). Contrasting interannual atmospheric CO$_2$ variabilities and their terrestrial mechanisms for two types of El Ninos. *Atmospheric Chemistry and Physics*, *18*(14), 10333–10345. https://doi.org/10.5194/acp-18-10333-2018

Wang, J., Zeng, N., Wang, M., Jiang, F., Wang, H., & Jiang, Z. (2018). Contrasting terrestrial carbon cycle responses to the 1997/98 and 2015/16 extreme El Niño events. *Earth System Dynamics*, *9*(1), 1–14. https://doi.org/10.5194/esd-9-1-2018

Wang, W., Ciais, P., Nemani, R., Canadell, J. G., Piao, S., Sitch, S., et al. (2013). Variations in atmospheric CO$_2$ growth rates coupled with tropical temperature. *Proceedings of the National Academy of Sciences*, *110*(32), 13061–13066. https://doi.org/10.1073/pnas.1219683110

Werner, C., Meredith, L. K., Ladd, S. N., Ingrisch, J., Kübert, A., van Haren, J., et al. (2021). Ecosystem fluxes during drought and recovery in an experimental forest. *Science*, *374*(6574), 1514–1518. https://doi.org/10.1126/science.abj6789

Wilcoxon, F. (1945). Individual comparisons by ranking methods. *Biometrics Bulletin*, *1*(6), 80–83. https://doi.org/10.2307/3001968

Wittmann, F., Schöngart, J., Montero, J. C., Motzer, T., Junk, W. J., Maria, T. F. P., et al. (2006). Tree species composition and diversity gradients in white-water forests across the Amazon Basin. *Journal of Biogeography*, *33*(8), 1334–1347. https://doi.org/10.1111/j.1365-2699.2006.01495.x

Yang, J., Tian, H., Pan, S., Chen, G., Zhang, B., & Dangal, S. (2018). Amazon drought and forest response: Largely reduced forest photosynthesis but slightly increased canopy greenness during the extreme drought of 2015/2016. *Global Change Biology*, *24*(5), 1919–1934. https://doi.org/10.1111/gcb.14056

Yuan, W. P., Zheng, Y., Piao, S., Ciais, P., Lombardozzi, D., Wang, Y., et al. (2019). Increased atmospheric vapor pressure deficit reduces global vegetation growth. *Science Advances*, *5*(8), eaax1396. https://doi.org/10.1126/sciadv.aax1396

Zeng, N., Mariotti, A., & Wetzel, P. (2005). Terrestrial mechanisms of interannual CO$_2$ variability. *Global Biogeochemical Cycles*, *19*(1), GB1016. https://doi.org/10.1029/2004gb002273

References From the Supporting Information

Baker, D. F., Doney, S. C., & Schimel, D. S. (2006). Variational data assimilation for atmospheric CO$_2$. *Tellus B: Chemical and Physical Meteorology*, *58*(5), 359–365. https://doi.org/10.3402/tellusb.v58i5.17022

Basu, S., Guerlet, S., Butz, A., Houweling, S., Hasekamp, O., Aben, I., et al. (2013). Global CO$_2$ fluxes estimated from GOSAT retrievals of total column CO$_2$. *Atmospheric Chemistry and Physics*, *13*(17), 8695–8717. https://doi.org/10.5194/acp-13-8695-2013

Chen, Z., Liu, J., Henze, D. K., Huntzinger, D. N., Wells, K. C., Sitch, S., et al. (2021). Linking global terrestrial CO$_2$ fluxes and environmental drivers: Inferences from the orbiting carbon Observatory 2 satellite and terrestrial biospheric models. *Atmospheric Chemistry and Physics*, *21*(9), 6663–6680. https://doi.org/10.5194/acp-21-6663-2021

Chevallier, F., Fisher, M., Peylin, P., Serrar, S., Bousquet, P., Bréon, F. M., et al. (2005). Inferring CO$_2$ sources and sinks from satellite observations: Method and application to TOVS data. *Journal of Geophysical Research*, *110*(D24), D24309. https://doi.org/10.1029/2005jd006390

Crowell, S. M. R., Randolph Kawa, S., Browell, E. V., Hammerling, D. M., Moore, B., Schaefer, K., & Doney, S. C. (2018). On the ability of space-based passive and active remote sensing Observations of CO$_2$ to detect flux perturbations to the carbon cycle. *Journal of Geophysical Research: Atmospheres*, *123*(2), 1460–1477. https://doi.org/10.1002/2017jd027836

Deng, F., Jones, D. B. A., O'Dell, C. W., Nassar, R., & Parazoo, N. C. (2016). Combining GOSAT XCO$_2$ observations over land and ocean to improve regional CO$_2$ flux estimates. *Journal of Geophysical Research: Atmospheres*, *121*(4), 1896–1913. https://doi.org/10.1002/2015jd024157

Jacobson, A. R., Schuldt, K. N., Miller, J. B., Oda, T., Tans, P., Mund, J., et al. (2020). *CarbonTracker CT2019B*. Model published 2020 by NOAA Earth System Research Laboratory, Global Monitoring Division. https://doi.org/10.25925/20201008

Liu, J., Baskaran, L., Bowman, K., Schimel, D., Bloom, A. A., Parazoo, N. C., et al. (2021). Carbon monitoring system flux net biosphere exchange 2020 (CMS-flux NBE 2020). *Earth System Science Data*, *13*(2), 299–330. https://doi.org/10.5194/essd-13-299-2021

Liu, Z., Zeng, N., Liu, Y., Kalnay, E., Asrar, G., Wu, B., et al. (2022). Improving the joint estimation of CO_2 and surface carbon fluxes using a Constrained Ensemble Kalman Filter in COLA (v1.0). *Geoscientific Model Development*, *15*(14), 5511–5528. https://doi.org/10.5194/gmd-15-5511-2022

Maksyutov, S., Oda, T., Saito, M., Janardanan, R., Belikov, D., Kaiser, J. W., et al. (2021). Technical note: A high-resolution inverse modelling technique for estimating surface CO_2 fluxes based on the NIES-TM–FLEXPART coupled transport model and its adjoint. *Atmospheric Chemistry and Physics*, *21*(2), 1245–1266. https://doi.org/10.5194/acp-21-1245-2021

Phillips, O. L., Aragão, L. E., Lewis, S. L., Fisher, J. B., Lloyd, J., López-González, G., et al. (2009). Drought sensitivity of the Amazon rainforest. *Science*, *323*(5919), 1344–1347. https://doi.org/10.1126/science.1164033

Rodell, M., Houser, P. R., Jambor, U., Gottschalck, J., Mitchell, K., Meng, C. J., et al. (2004). The global land data assimilation system. *Bulletin America Meteorology Social*, *85*(3), 381–394. https://doi.org/10.1175/bams-85-3-381

Schuh, A. E., Denning, A. S., Corbin, K. D., Baker, I. T., Uliasz, M., Parazoo, N., et al. (2010). A regional high-resolution carbon flux inversion of North America for 2004. *Biogeosciences*, *7*(5), 1625–1644. https://doi.org/10.5194/bg-7-1625-2010

Sungmin, O., & Orth, R. (2021). Global soil moisture data derived through machine learning trained with in-situ measurements. *Scientific Data*, *8*(1), 170. https://doi.org/10.1038/s41597-021-00964-1

Zammit-Mangion, A., Bertolacci, M., Fisher, J., Stavert, A., Rigby, M., Cao, Y., & Cressie, N. (2022). WOMBAT v1.0: A fully Bayesian global flux-inversion framework. *Geoscientific Model Development*, *15*(1), 45–73. https://doi.org/10.5194/gmd-15-45-2022